

Atomistic Simulations in Nanostructures Composed of Tens of Millions of Atoms: Importance of long-range Strain Effects in Quantum Dots

M. Korkusinski¹, G. Klimeck^{1,2}, H. Xu¹, S. Lee², S. Goasguen¹, and F. Saied¹,

¹Purdue University, West Lafayette, IN, 47907, USA, marekk@purdue.edu

²Jet Propulsion Laboratory, California Institute of Technology, Pasadena, CA, 91109, USA

ABSTRACT

Strain in self-assembled quantum dots is a long-range phenomenon, and its realistic determination requires a large computational domain. To tackle this problem for an embedded InAs quantum dot NEMO-3D uses the atomistic VFF Keating model containing up to 64 million atoms. Interatomic distance changes obtained are used to influence the $sp^3d^5s^*$ tight-binding electronic Hamiltonian defined in a subdomain containing up to 21 million atoms (matrix size of order of 4×10^8). Targeted eigenstates with correct symmetry are found reliably even in such large systems. NEMO-3D is used to analyze the dependence of the dot states on the size of the strain domain and the boundary conditions. The energies of a deeply embedded dot depend dramatically on the strain domain size. For dots buried under a thin capping layer, on the other hand, the existence of a free surface at the top of the sample allows for an effective relaxation of atoms, and the penetration of strain into the barrier is small.

Keywords: nanoelectronics, quantum dots, atomistic simulations, strain, electronic structure, parallel computing, tight binding

1 INTRODUCTION

Quantum dots (QDs) are solid-state structures capable of trapping charged carriers so that their wave functions become fully spatially localized, and their energy spectra consist of well-separated, discrete levels. Existing nanofabrication techniques make it possible to manufacture QDs in a variety of types and sizes [1]. Among them, semiconductor QDs grown by self-assembly (SADs), trapping both electrons and holes, are of particular importance in quantum optics, since they can be used as detectors of infrared radiation [2], optical memories [3], single photon sources [4]. Arrays of quantum-mechanically coupled SADs can also be used as optically active regions in high-efficiency, room-temperature lasers [5].

The self-assembly of SADs is achieved in the Stranski-Krastanow growth mode [6] as a result of the mismatch of lattice constants of the material of the dot (e.g., InAs) and that of the substrate semiconductor (e.g., GaAs). This mismatch leads to the appearance of a long-range strain field, which strongly modifies the energy diagram of the system [7]. Therefore, device simulations must include the

fundamental quantum character of charge carriers and the classical, long-distance strain effects on equal footing. The Nanoelectronic Modeling tool NEMO-3D [8] meets these requirements by modeling the strain and electronic structure of extended nanosystems (on the length scale of tens of nanometers, containing tens of millions of atoms) fully on the atomistic level.

This work reports on the application of NEMO-3D to study the impact of the strain on the electronic structure of a SAD. The first part of the paper gives a brief summary of NEMO-3D and its performance on parallel computing platforms. In the second part, NEMO-3D is used to study the sensitivity of the single SAD's energy spectrum to the size and boundary conditions of the strain domain, as well as to the geometry of the sample, the thickness of the capping layer and the distance between neighboring SADs in lateral quantum-dot arrays.

2 SYSTEM AND METHOD

2.1 Physical Structure

InAs dome-shaped QDs with diameter and height respectively of 18.09 nm and 1.7 nm (dot A) and 27.13 nm and 2.54 nm (dot B), positioned on a 0.6-nm-thick wetting layer, and embedded in the GaAs barrier material (Fig. 1) are considered. The computational strain domain denoted by lateral size d and vertical size h , can be much larger than the electronic structure domain (Fig. 1).

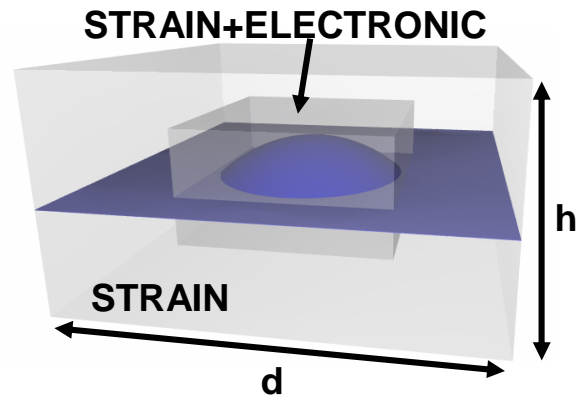


Fig. 1. Schematic view of the QD nanostructure, with two simulation domains: central for electronic structure, and larger for strain calculations

In the electronic calculation, only the confined states are targeted. Since their wave functions decay exponentially in the barrier, it is sufficient to consider a smaller computational box, as shown in Fig. 1.

2.2 NEMO-3D: Overview and Performance

NEMO-3D is an atomistic simulation tool designed to provide *quantitative* predictions of the electronic structure of nanodevices [8, 9]. The computation consists of two major steps. First, the strain distribution in the device is found by computing the positions of atoms yielding the minimal total elastic energy. Contributions to that energy from each distorted atomic bond are obtained in the frame of the valence-force-field method with Keating potentials, and the minimization procedure employs the conjugate gradient technique. In the second step, an atomistic tight-binding Hamiltonian is used to find the electron and hole energy levels and wave functions of the system. This Hamiltonian is created in the basis of 20 orbitals per atom (spin-degenerate s, p, d, and s*). Interactions between the orbitals within each atom and between the nearest neighbors are empirical fitting parameters, chosen so that the model reproduces the experimentally measured band structure of bulk semiconductors. Further, the tight-binding parameters are functions of interatomic bond length and angle distortions due to strain. The resulting Hamiltonian matrix is sparse; targeted eigenvalues and eigenvectors are found using the Lanczos algorithm.

Proper treatment of strain requires computational domains of tens of millions atoms. The electronic domains are usually smaller (up to 20 million atoms), but the sp3d5s* basis set results in Hamiltonian matrices of order of 20 times that number. Therefore, parallelization of NEMO-3D is a key consideration. The core computational engine of NEMO-3D was written in C with MPI used for message passing, which ensures its portability across major parallel computing platforms. Figure 2 shows the memory usage per CPU in the strain (a) and electronic part (b) as a function of the number of CPUs and the system's size. Both phases scale well for a small number of CPUs, but the strain part exhibits a saturation tendency for larger number of CPUs. This is due to a relatively large contribution of non-parallelizable data structures containing system information to the total memory occupied in this phase. In the electronic computation the memory usage is dominated by parallelizable data structures of the Lanczos algorithm, which results in a better scaling behavior.

The Lanczos procedure is particularly computationally challenging because (i) the spectrum of the Hamiltonian has a gap in its interior, and the sought eigenvalues lie above and below this gap; (ii) the eigenvalues are typically repeated, since at zero magnetic field the spin-up and spin-down electronic states are degenerate; (ii) the corresponding eigenvectors are effectively nonzero only on

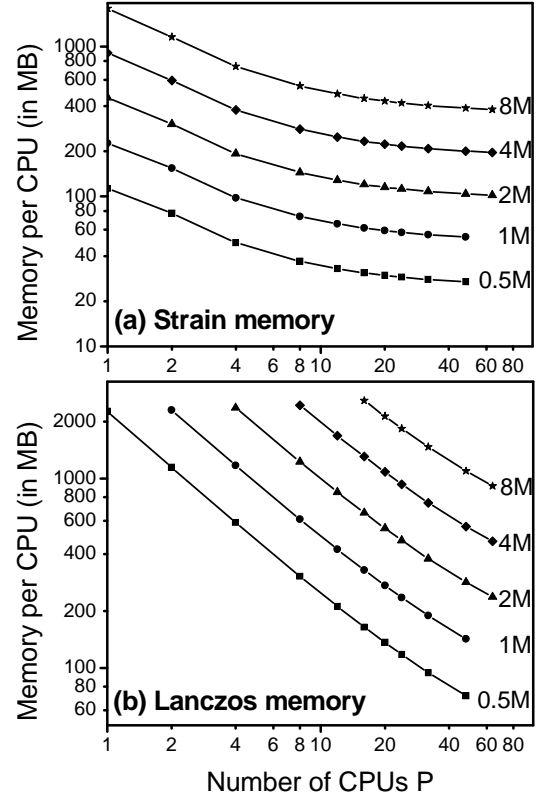


Fig. 2. Memory per CPU in the strain (a) and electronic (b) part of NEMO simulation as a function of the number of CPUs (P) for systems with 0.5 - 8 million atoms.

a small subset (a few tens of thousands of atoms) of the multimillion-atom domain. Therefore it is essential to prove that unique and targeted eigenstates can be extracted from the spectrum. Figure 3 shows a 2D slice through the electronic ground-state probability density for the same QD (dot A), but with the electronic domain containing 300 000 (a) and 21 million atoms (b). As can be seen, the orbital retains its unique, correct symmetry even for the largest electronic computational domain. The computational time in the electronic phase scales nearly linearly with the number of atoms, as demonstrated in Fig. 3 (c). A computation of four electronic and four hole eigenstates of a 21-million-atom domain takes about 12 hours on 64 Itanium 2 CPUs (1.5 GHz).

3 STUDY OF STRAIN IN SADS

3.1 Sensitivity to Size of the Strain Domain

The first NEMO-3D simulation of the SAD examines the sensitivity of its electronic levels on the size and boundary conditions of the strain domain. This first study

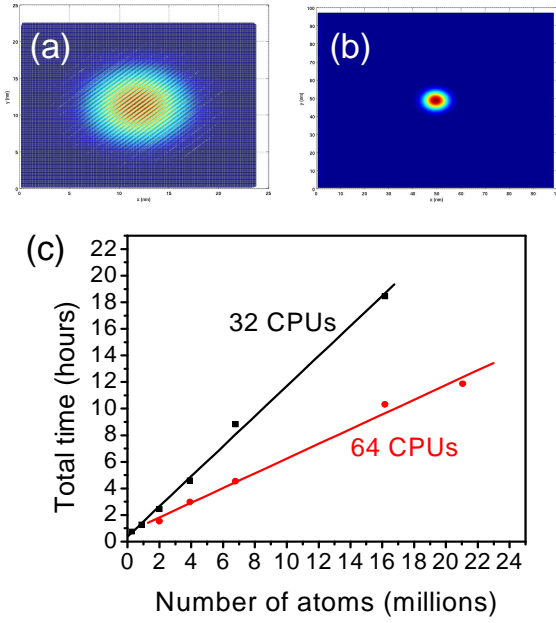


Fig. 3. Probability density for the electronic ground state computed with the computational domain containing (a) 300 000 and (b) 21 million atoms. (c) Total time of the Hamiltonian diagonalization versus system size on 32 and 64 CPUs of an Itanium 2 cluster.

treats a deeply embedded dot A, where the size of the strain domain around it is increased in all directions. Its volume is taken to contain from 2 to 64 million atoms, and its aspect ratio is fixed so that $d/h = 2$. Also, two sets of boundary conditions are used. In the first set the positions of all the atoms on the domain boundary are fixed to GaAs bulk positions (fixed BCs). In the second set only the bottom boundary is fixed; periodic conditions are assumed in the XY plane, and the top is free (mixed BCs). Once the strain calculation is completed, the electronic calculation is carried out on a 2-million-atom domain with fixed boundary conditions. Figure 4 shows the ground and two excited states for the electron and the hole as a function of the size d . The size of the strain domain influences the electronic levels dramatically, particularly for fixed BCs, where the convergence is not achieved even for the largest domain size. Much faster convergence is obtained for mixed BCs, which better reflect the actual physical setup of SAD arrays (the underlying substrate fixes the bottom of the domain and the SADs are covered with a capping layer of finite thickness, so that the elastic energy can be minimized by distorting the top surface). The mixed BCs are employed in the remainder of this work.

3.2 Strain Sensitivity to QD Shape

The height of the SAD is much smaller than its diameter. One might thus expect that the lateral extent of

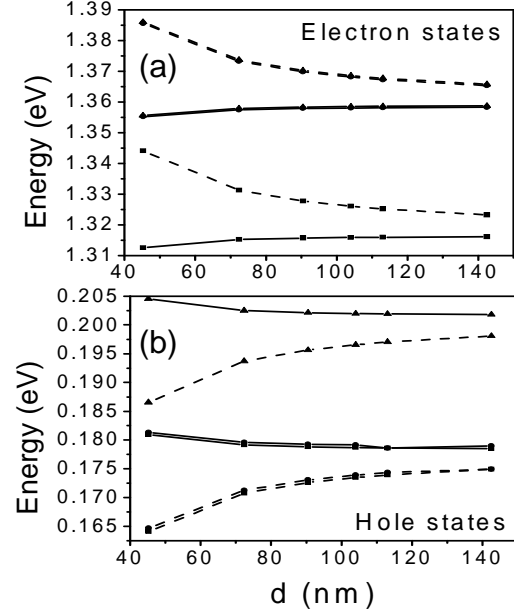


Fig. 4. Electronic (a) and hole (b) ground and two excited energy levels of dot A as a function of the lateral size d of the strain domain with mixed (solid lines) and fixed (dashed lines) BCs. In this calculation the ratio $d/h=2$.

the strain field caused the QD might be different than its vertical extent. To verify this, a study similar to that presented in the previous Section was conducted with the strain domain aspect ratio set to $d/h = 0.5$, i.e., the domain is now a pillar, whose height is twice larger than its base length. Figure 5 shows a comparison of the electron (a) and hole (b) energies as a function of the size d for the two aspect ratios. The convergence is much faster for the pillar-shaped strain domain, which indicates that the strain field caused by the SAD has a dominant vertical component, whose penetration depth into the barrier is much larger than that in the XY plane. This observation is in agreement with the experimentally observed strain-induced stacking of SADs grown in vertical layers [10].

In the mixed BCs the top boundary of the strain domain is not fixed, and periodic boundary conditions are assumed on its side walls, which corresponds well to the experimental conditions. Care must be taken, however, with the bottom boundary of the strain domain, because positions of atoms placed on it are fixed to the bulk substrate positions. To justify this assumption, the strain domain must extend sufficiently far below the SAD structure. A convergence study of the electronic levels (not shown here) indicates that the distance from the bottom boundary to the bottom of the wetting layer has to be at least 55.4 nm for dot A, and at least 78.01 nm for dot B.

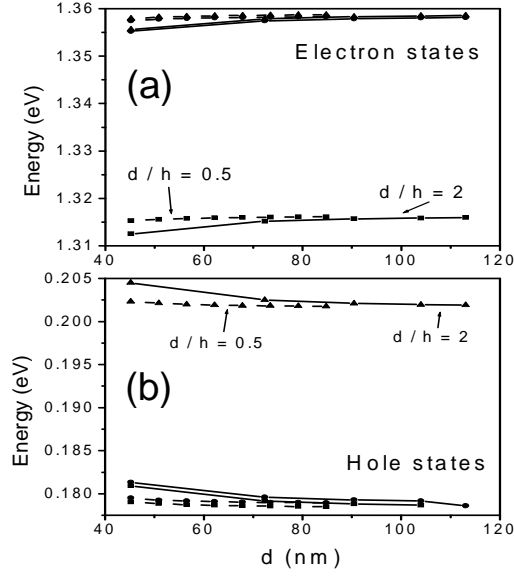


Fig. 5. Electronic (a) and hole (b) ground and two excited energy levels of the dot A as a function of the lateral size d of the strain domain for the aspect ratio $d/h=2$ (solid lines) and $d/h=0.5$ (dashed lines). Mixed BCs are used.

3.3 Effect of Finite Capping Layer

Experiments probe SADs buried under a finite capping layer. To reproduce these conditions, in this study the capping layer thickness c , measured from the top of the wetting layer to the top boundary of the strain domain, is treated as a parameter and fixed. Periodic BCs are taken in the XY plane for both strain and electronic calculations (the side domain boundaries in both of them coincide), so that arrays of SADs, laterally coupled both via the classical strain field and quantum-mechanically, are studied.

Fig. 6 shows the electronic and hole ground states of an infinite SAD array as functions of the interdot distance b (measured from dot edge to edge) for several cap thicknesses c and for dots A (top panels) and B (bottom panels). In both cases the energies clearly depend on the interdot distance. For thicker cap layers the effective semiconductor gap increases with the increase of b , to reach saturation when SADs are far apart. For the thinnest caps, however, a nonmonotonic behavior is observed for the electronic ground state (it is seen particularly clearly for dots A in Fig. 6 (a)). For fixed b the effective gap increases as the cap thickness c increases, to reach saturation for thick capping layers (in accordance with Fig. 5). For $b = 30$ nm and c changing by about 10 nm, the total effective gap increases by about 7.5 meV.

Acknowledgements

The work described in this publication was carried out in part at the Jet Propulsion Laboratory, California Institute of

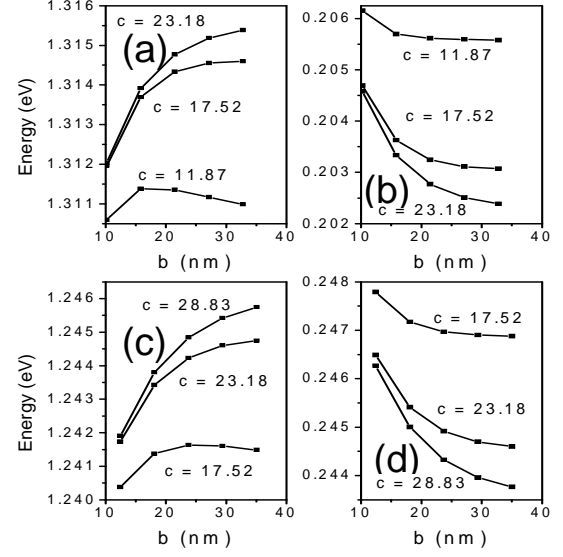


Fig. 6. Electronic (a, c) and hole (b, d) ground-state energies for dot arrays composed of dots A (top) and dots B (bottom) as a function of the distance b between SADs for different capping layer thicknesses c (given in nm).

Technology under a contract with the National Aeronautics and Space Administration. Funding at Purdue was provided by NSF under Grant No. EEC-0228390 and by the Indiana 21st Century Fund. At JPL funding was provided under grants from ONR, ARDA, and JPL.

REFERENCES

- [1] For reviews and references see, e.g., Jacak, L., Hawrylak, P., and Wojs, A., "Quantum dots", Springer-Verlag, Berlin, 1998.
- [2] Aslan, B., Liu, H.C., Korkusinski, M., Cheng, S.-J., and Hawrylak, P., Appl. Phys. Lett., 82, 630, 2003.
- [3] Petroff, P.M., in "Single Quantum Dots: Fundamentals, Applications, and New Concepts", Peter Michler, Ed., Springer, Berlin, 2003.
- [4] Michler, P., et al., Science, 290, 2282, 2000; Moreau, E., et al., Phys. Rev. Lett., 87, 183601, 2001.
- [5] Arakawa, Y., and Sasaki, H., Appl. Phys. Lett., 40, 939, 1982; Fafard, S., et al., Science, 22, 1350, 1996; Maximov, M.V., et al., J. Appl. Phys., 83, 5561, 1998.
- [6] Petroff, P.M. and DenBaars, S.P., Superlatt. Microstruct. 15, 15, 1994.
- [7] For a review and references see, e.g., Tadic, M., et al., J. Appl. Phys. 92, 5819, 2002.
- [8] Klimeck, G., et al., Computer Modeling in Engineering and Science, 3, 601, 2002.
- [9] Oyafuso, F., et al., Journal of Computational Electronics, 1, 317, 2002.
- [10] Wasilewski, Z.R., Fafard, S., and McCaffrey, J.P., J. Cryst. Growth, 201, 1131, 1999.